Upper tropospheric ozone derived from the cloud slicing technique: Implications for large-scale convection

J. R. Ziemke

Goddard Earth Sciences and Technology (GEST) Center, University of Maryland Baltimore County, Baltimore, Maryland, USA

NASA Goddard Space Flight Center, Greenbelt, Maryland, USA

S. Chandra and P. K. Bhartia

NASA Goddard Space Flight Center, Greenbelt, Maryland, USA

Received 6 September 2002; revised 13 March 2003; accepted 24 March 2003; published 10 July 2003.

[1] This study evaluates the spatial distributions and seasonal cycles in upper tropospheric ozone (pressure range 200–500 hPa) from low to high latitudes (60°S to 60°N) derived from the satellite retrieval method called "cloud slicing." The cloud slicing method determines ozone profile information in the troposphere by combining colocated measurements of cloud top pressure and above-cloud column ozone. Measurements of Nimbus 7 Total Ozone Mapping Spectrometer (TOMS) above-cloud column ozone and Nimbus 7 Temperature Humidity Infrared Radiometer (THIR) cloud top pressure during 1979–1984 were merged to derive upper tropospheric ozone. Because of large footprint measurements from TOMS (~100 km diameter on average), upper tropospheric ozone derived from cloud slicing coincides with large-scale convection events. These events are not necessarily representative of average atmospheric conditions in regions near and poleward of the tropospheric wind jets (around ±30° latitude), especially in winter and spring seasons when dynamical wave activity in the troposphere and lower stratosphere is most intense. The cloud slicing method with Nimbus 7 geometry in any case provides a unique opportunity to investigate the behavior of upper tropospheric ozone under condition of intense broad-scale convection. In the tropics the measured upper tropospheric ozone shows year-round enhancement in the Atlantic region and evidence of a possible semiannual variability. Outside the tropics, upper tropospheric ozone from cloud slicing shows greatest abundance in winter and spring seasons in both hemispheres with largest variance and largest amounts in the northern hemisphere. This seasonal cycle behavior under conditions of intense convection is different from general ozonesonde climatology which shows instead upper tropospheric ozone maximizing around early to middle summer months. The seasonal cycles and spatial characteristics in upper tropospheric ozone from cloud slicing are similar to lower stratospheric ozone. It is suggested that the large-scale convection events with cloud slicing coincide with an occurrence of stratosphere-troposphere exchange (STE). *INDEX TERMS:* 0365 Atmospheric Composition and Structure: Troposphere—composition and chemistry; 0368 Atmospheric Composition and Structure: Troposphere—constituent transport and chemistry; 3309 Meteorology and Atmospheric Dynamics: Climatology (1620); 3360 Meteorology and Atmospheric Dynamics: Remote sensing; 3362 Meteorology and Atmospheric Dynamics: Stratosphere/troposphere interactions; *KEYWORDS:* cloud slicing, tropospheric ozone, STE, THIR

Citation: Ziemke, J. R., S. Chandra, and P. K. Bhartia, Upper tropospheric ozone derived from the cloud slicing technique: Implications for large-scale convection, *J. Geophys. Res.*, *108*(D13), 4390, doi:10.1029/2002JD002919, 2003.

1. Introduction

[2] The first assessment of tropospheric column ozone (TCO) derived from satellite measurements was based on the residual method of *Fishman et al.* [1990] which subtracted SAGE stratospheric column ozone (SCO) from TOMS total column ozone to determine TCO. Although it was demonstrated that this method could retrieve information of TCO distributions extending from the tropics to middle latitudes, essentially only a climatology of TCO was obtainable because of the sparse solar occultation measurements of stratospheric ozone profiles available from SAGE. The SAGE instrument makes around 15 sunrise

0148-0227/03/2002JD002919$09.00

and 15 sunset profile measurements per day which over a month provide about 900 measurements and near global coverage. In addition it was noted by *Fishman et al.* [1990] that this method had further difficulties caused by subtracting two large column ozone measurements from two independent instruments (i.e., TOMS and SAGE) which were not inter-calibrated.

[3] Subsequently, a number of algorithms based on tropospheric ozone residual methods were developed with significant improvements in characterizing the seasonal, interannual, and spatial variations of TCO in the tropics [e.g., *Jiang and Yung*, 1996; *Kim and Newchurch*, 1996; *Hudson and Thompson*, 1998; *Ziemke et al.*, 1998; *Ziemke and Chandra*, 1999; *Thompson and Hudson*, 1999; *Fishman and Balok*, 1999; *Kim et al.*, 2001; *Ziemke et al.*, 2001; *Chandra et al.*, 2003]. The TCO derived from these techniques have yielded many important scientific results including characterization of ozone enhancement in the Atlantic during southern spring (first identified by *Fishman and Larsen* [1987]), evidence of an El Nino signal [*Chandra et al.*, 1998; *Thompson and Hudson*, 1999], solar cycle forcing [*Chandra et al.*, 1999], characterization of seasonal and interannual variabilities [*Ziemke and Chandra*, 1999], and identification of lightning-generated TCO distributions [*Martin et al.*, 2001]. Additional studies have shown that the September–October Atlantic maximum and/or the El Nino increase of tropospheric ozone over Indonesia in 1997 were well captured in 3D photochemical transport models [e.g., *Moxim and Levy*, 2000; *Sudo and Takahashi*, 2001; *Bey et al.*, 2001; *Martin et al.*, 2002; *Chandra et al.*, 2002].

[4] While much has been learned about tropical TCO from various satellite retrieval methods, the extension of measurements and the characterization of TCO outside the tropics has had limited success. The residual method of *Fishman et al.* [1990] was more recently applied by replacing SAGE measurements with solar backscatter ultraviolet (SBUV) to determine SCO [*Vukovich et al.*, 1996; *Fishman and Balok*, 1999]. Unlike SAGE the SBUV profiles provide daily measurements of SCO over much of the globe. However SCO derived from SBUV has had limited success because of poor vertical resolution of ozone profile information in the vicinity of the tropopause. *Fishman and Balok* [1999] provided an improvement to this TOMS/SBUV residual technique by applying a normalization to the SBUV profile measurements using ozonesonde climatology [*Logan*, 1999]. Recently, *Chandra et al.* [2003] applied a new cross-calibration technique to TOMS total ozone and Microwave Limb Sounder (MLS) stratospheric column ozone to derive several years of high-resolution TCO maps.

[5] The cloud slicing technique [*Ziemke et al.*, 2001] provides a method for deriving ozone in the upper troposphere over much of the Earth wherever sufficient clouds exist and colocated measurements of above-cloud column ozone and cloud-top pressures are available. The Nimbus 7 TOMS instrument determines total column ozone in the atmosphere from measuring backscattered UV radiances at six wavelengths varying from 313 nm to 380 nm. Optically thick water vapor clouds in the troposphere are opaque at these UV wavelengths, and as a result the column ozone amount actually measured by TOMS in the presence of such clouds is ''above-cloud'' column ozone. The general scheme behind cloud slicing is that it takes advantage of the opaque nature of thick clouds and above-cloud column ozone measurements to estimate ozone abundance in the troposphere. With this method, above-cloud column ozone is plotted versus colocated cloud-top pressure for a chosen geographical region and for a preselected pressure band. The mean slope of the distribution directly yields mean ozone volume mixing ratio. Since the method uses only tropospheric clouds, the ozone measured is assured to always lie below the tropopause. We note that the footprint measurements from Nimbus 7 TOMS are $\sim$100 km diameter on average. As a result, upper tropospheric ozone derived from cloud slicing coincides with intense large-scale convection events. Events such as these are not necessarily representative of average atmospheric conditions in regions near and poleward of the tropospheric wind jets (around $\pm 30^\circ$ latitude). This is especially evident in winter and spring seasons in the extratropics when dynamical wave activity in the troposphere and lower stratosphere is most intense and can vary greatly from average climatological conditions [e.g., *Randel*, 1992]. The cloud slicing method applied to Nimbus 7 data nevertheless provides a unique opportunity to characterize the spatial distributions and temporal behavior of upper tropospheric ozone under the condition of intense large-scale convection on a near-global nature.

[6] The current study investigates upper tropospheric ozone volume mixing ratio from cloud slicing in the pressure range 200–500 hPa between latitudes 60°S to 60°N and characterizes both spatial patterns and seasonal variabilities present in the data. Although not the main objective, we also investigate possible implications for stratosphere-troposphere exchange (STE) by comparing spatial distributions and seasonal cycles in upper tropospheric ozone with lower stratospheric ozone from UARS Halogen Occultation Experiment (HALOE), TOMS total column ozone measurements, and lower stratospheric air mass derived from NCEP reanalyses. Ozone in the upper troposphere and lower stratosphere exhibits lifetimes of months to years, respectively. In these regions ozone is a chemical tracer of air mass motion and distribution. Upper tropospheric ozone derived from Nimbus 7 cloud slicing coincides with dynamically intense broad-scale convection events. One may expect that upper tropospheric ozone, lower stratospheric ozone, and lower stratospheric air mass will show similar seasonal cycles with the occurrence of STE.

[7] The following sections begin with a description of the data and an overview of the cloud slicing method, followed by ozonesonde comparison of measurements, characterization of seasonal cycles and spatial distributions, correlations of seasonal cycles, and finally a summary.

2. Nimbus 7 Data and Cloud Slicing

[8] Nimbus 7 Temperature Humidity and Infrared Radiometer (THIR) cloud-top pressure and Nimbus 7 TOMS version 7 column ozone level-2 footprint measurements were combined to determine upper tropospheric ozone from the method of cloud slicing [*Ziemke et al.*, 2001]. The THIR instrument provides thermal emission measurements in a 2 μm-wide channel centered about 11.5 μm to determine

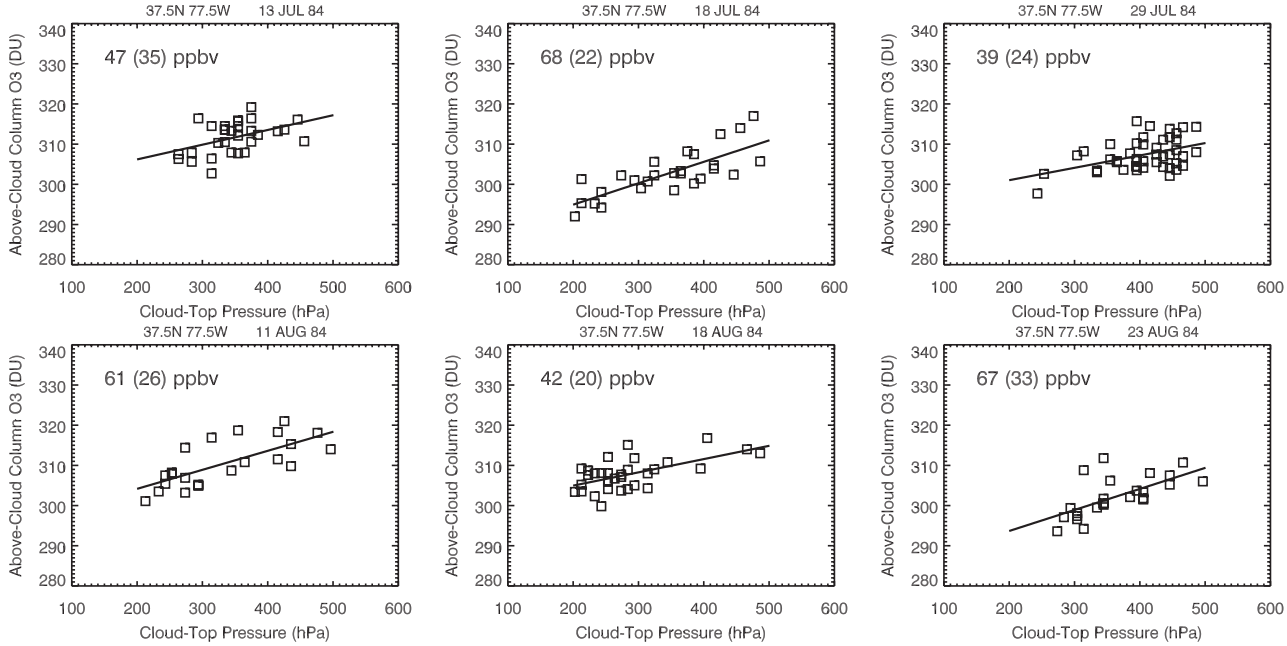

Figure 1. Scatterplots of TOMS above-cloud column ozone (in Dobson units) versus colocated THIR cloud top pressure (in hPa) for a grid point located near Wallops, Virginia (38°N, 75°W). The top three frames are three days in July 1984, and the bottom three frames are days in August 1984. The numbers shown in each scatterplot are the derived ozone volume mixing ratio and 2-σ uncertainties (in parentheses) in units ppbv.

cloud-top temperature. THIR cloud-top pressure was derived from temperature using National Centers for Environmental Prediction (NCEP) analyses. Monthly ensemble averages from cloud slicing were derived from daily values from January 1979 through October 1984 between latitudes 60°S and 60°N (5° × 5° resolution). The pressure band for cloud slicing was chosen following several trial data runs to be 200–500 hPa to optimize both number of measurements and signal-to-noise. In tropical latitudes the tropopause lies around 100 hPa year-round while in middle and high latitudes the tropopause may lie at 300 hPa or greater pressure in winter or spring. cloud slicing measurements represent mean ozone volume mixing ratio in the upper troposphere lying between 500 hPa and highest cloud tops limited to 200 hPa in THIR cloud pressure data. The 200–500 hPa band in the tropics and lower subtropics represents the middle to upper troposphere. In higher latitudes it is mostly the upper troposphere.

[9] It is important to comment further regarding the 200–500 hPa pressure band that we selected for cloud slicing. First, there are errors present in the absolute measurements of THIR cloud-top pressures. The study by *Newchurch et al.* [2001] used 2 months of reprocessed THIR cloud-top pressure data to adjust the 1979–1984 THIR level-2 cloud-top pressure data used in this study. *Newchurch et al.* [2001, Figure 1] indicated that the reprocessed THIR values were larger by 50–100 hPa for unadjusted level-2 THIR pressures in the vicinity of 100 hPa in the northern tropics (0–10N). In this study we analyzed the most recent database of reprocessed THIR data (508 selected days over time frame 1979–1984) and found average adjustments to level 2 THIR of around +50 hPa for pressure range 200–500 hPa and for latitude range 60°S to 60°N. We did not attempt to use the reprocessed THIR directly for cloud slicing, only to provide estimated adjustments to level 2 THIR cloud-top pressures. The main difficulties with directly using revised THIR data for cloud Slicing are (1) only 508 days are currently available, and (2) the data formatting is not the same as standard level-2 formatting which makes accurate space-time colocation of cloud slicing data pairs cumbersome. We concluded that it is possible that the 200–500 hPa pressure band in level 2 THIR data for 60°S to 60°N may be more likely around 250–550 hPa.

[10] We note that because cloud slicing uses tropospheric clouds, all measurements of ozone from cloud slicing lie below the tropopause. This is true regardless of geographical position or the time of season. However, we cannot rule out the possibility that the ozone detected from cloud slicing below the tropopause may actually have a stratospheric origin because of the intense broad-scale convection/dynamics associated with Nimbus 7 cloud slicing. Further details for the cloud slicing algorithm are discussed in Appendix A.

[11] Figure 1 shows scatterplots of TOMS above-cloud column ozone versus colocated THIR cloud-top pressure for a grid point located near Wallops, Virginia (38°N, 75°W). The top three frames are three days in July 1984 and the bottom three frames are days in August 1984. The numbers shown in each scatterplot are the derived ozone volume mixing ratio and 2σ uncertainties (in parentheses) in units ppmv. The best cases/statistics are usually in summer and autumn when it is common to obtain several daily cloud slicing measurements for a given month. There are usually more measurements in summer and autumn than in winter and spring. Part of the reason for more measurements in summer and autumn is less ozone variability in the strato-

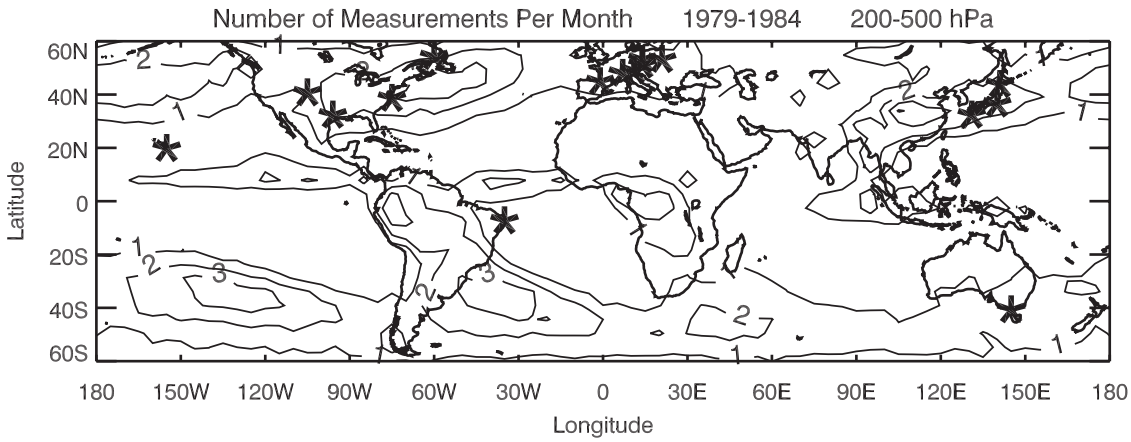

Figure 2. Average number of cloud slicing measurements per month in this. Large asterisks denote sonde locations used in this study for comparisons.

sphere and the 2σ statistical filtering used in cloud slicing (see Appendix A). The scatter in the distributions in Figure 1 is caused by errors in TOMS above-cloud column measurements and also errors caused by some amount of stratospheric ozone variability over the selected 5° × 5° region (discussed in the Appendix). Some additional scatter in the plots in Figure 1 is caused by errors in converting THIR cloud-top temperature measurements to pressure using NCEP analyses. Future satellite instruments with greater spectral resolution may enable the determination of cloud-top pressure directly instead of having to convert measured cloud-top temperature to pressure from meteorological analyses. Methods capable of deriving the tropopause directly from backscattered UV and visible wavelength radiances include the molecular oxygen dimer (O2-O2) method (J. Joiner and S. Vasilkov, personal communication, 2002–2003) and the rotational Raman scattering ''ring effect'' [*Joiner and Bhartia*, 1995].

[12] Figure 2 shows the average number of cloud slicing measurements per month in this investigation. Some regions have average monthly sampling rates 1–2, with a few other regions up to around 3. These numbers are small, yet still comparable to many ground-based ozonesonde stations (section 3). There are two regions in Figure 2 where there are no measurements at all from Nimbus 7 cloud slicing because of an insufficient number of high clouds or high reflectivity scenes: (1) the south Pacific oceanic region west of South America, and (2) the south Atlantic oceanic region lying between South America and Africa.

3. Comparisons With Ozonesonde Measurements

[13] Time series of upper tropospheric ozone from cloud slicing were compared with similar time series at several ground-based World Ozone and Ultraviolet Radiation Data Center (WOUDC) stations. Comparisons with the sonde data indicate that the cloud slicing scenes likely coincide with highly dynamical convective events with a high tropopause. In this discussion we refer to Tables 1 and 2, which were derived from the seasonal cycles between cloud slicing and ozonesondes. When we first compared seasonal cycles in mean mixing ratio between ozonesondes (500 hPa to tropopause) and cloud slicing, we found that the agreement was not good. Table 1 summarizes this result for several WOUDC station sites, giving mean offset differences and correlations of seasonal cycles. Next, when we prefiltered the sonde data to ensure that the cold-point tropopause pressure was less than 200 hPa the comparisons were improved, not necessarily in mean offsets but the basic seasonal correlations between the two data sources improved significantly. This result is summarized in Table 2. We note that filtering does not significantly alter the sonde measurements equatorward of the tropospheric wind jets (i.e., around 30° in both hemispheres). In these regions the tropopause pressure is usually less than 200 hPa year-round (e.g., compare Table 1 and Table 2 for Hilo (20°N, 155°W)).

[14] All ozonesonde data plotted in this study were prefiltered for cold-point tropopause pressures less than 200 hPa. Temperature profiles used were from in situ sonde measurements. In the atmosphere, temperature decreases with altitude in the troposphere and increases with altitude in the stratosphere. The cold-point tropopause pressure was determined from the minimum temperature (cold-point) between these two regimes. We note that there are other definitions of the tropopause such as in terms of potential vorticity or the 2K per km lapse rate condition [e.g., *Logan*,

Table 1. Offset Difference (Cloud Slicing Minus Sonde) in Upper Tropospheric Ozone and Seasonal-Cycle Correlation Between the Two Series[a]

Station	Offset/Correlation
Goose (53°N, 60°W)	13/−0.12
Lindenberg (52°N, 14°E)	−10/0.77
Legionowo (52°N, 21°E)	−2/0.43
Praha (50°N, 14°E)	−12/0.36
Hohenpeissenberg (48°N, 11°E)	5/0.47
Payerne (47°N, 7°E)	−9/−0.16
Biscarrosse (44°N, °W)	−3/0.18
Sapporo (43°N 141°E)	22/−0.51
Boulder (40°N 105°W)	8/0.21
Wallops (38°N, 75°W)	−12/0.25
Tateno (36°N 140°E)	−1/0.18
Kagoshima (32°N 131°E)	−4/0.27
Palestine (32°N 96°W)	−9/0.28
Hilo (20°N 155°W)	−3/0.62
Natal (6°S, 35°W)	−26/0.27
Laverton (38°S 145°E)	6/0.34

[a]Mean upper tropospheric ozone was derived as mean mixing ratio between 500 hPa and existing tropopause. Correlation amplitudes exceeding 0.58 pass 95% confidence level (i.e., 5% significance level). Units are ppbv.

Table 2. Same as Table 1 But With Constraint That the Tropopause Pressure be Less Than 200 hPa

Station	Offset/Correlation
Goose (53°N, 60°W)	−5/0.19
Lindenberg (52°N, 14°E)	−14/0.74
Legionowo (52°N, 21°E)	−7/0.67
Praha (50°N, 14°E)	−10/0.70
Hohenpeissenberg (48°N, 11°E)	2/0.80
Payerne (47°N, 7°E)	−4/0.48
Biscarrosse (44°N, 1°W)	5/0.33
Sapporo (43°N 141°E)	19/0.60
Boulder (40°N 105°W)	10/0.53
Wallops (38°N, 75°W)	−4/0.66
Tateno (36°N 140°E)	8/0.72
Kagoshima (32°N 131°E)	5/0.27
Palestine (32°N 96°W)	3/0.87
Hilo (20°N 155°W)	6/0.59
Natal (6°S, 35°W)	−19/0.48
Laverton (38°S 145°E)	8/0.78

1999, and references therein]. Analyses of NCEP data for cold-point and 2K per km definitions shows that generally the difference in tropopause pressure between these definitions is small (only a few hPa) in the tropics, but can at times be large (even exceeding 50 hPa) in middle and higher latitudes (figures not shown). We note that for sonde data there are occasions when the tropopause defined from cold-point also lies significantly above the 2K per km lapse-rate tropopause and where there is a rapid increase in ozone. Under conditions of high altitude tropopause and intense convective dynamics/high clouds, it may be possible that some of this ozone is being measured in the troposphere from cloud slicing. It is noted that under extreme dynamical conditions the determination of the tropopause itself becomes difficult and subjective depending on the definition of tropopause used (e.g., in terms of potential vorticity, lapse rate value, cold-point temperature, etc.).

[15] It may not be possible to make a true comparison between ozonesondes and Nimbus 7 cloud slicing regardless of how the ozonesonde data are prefiltered. Measurements from Nimbus 7 are large scenes (∼100 km footprint diameter on average) and coincide with highly dynamical events (i.e., many huge convective cells over a broad region). These convective events are generally unique. This is a limitation of current cloud slicing from Nimbus 7. Smaller FOV measurements (13 km × 24 km at Nadir) from

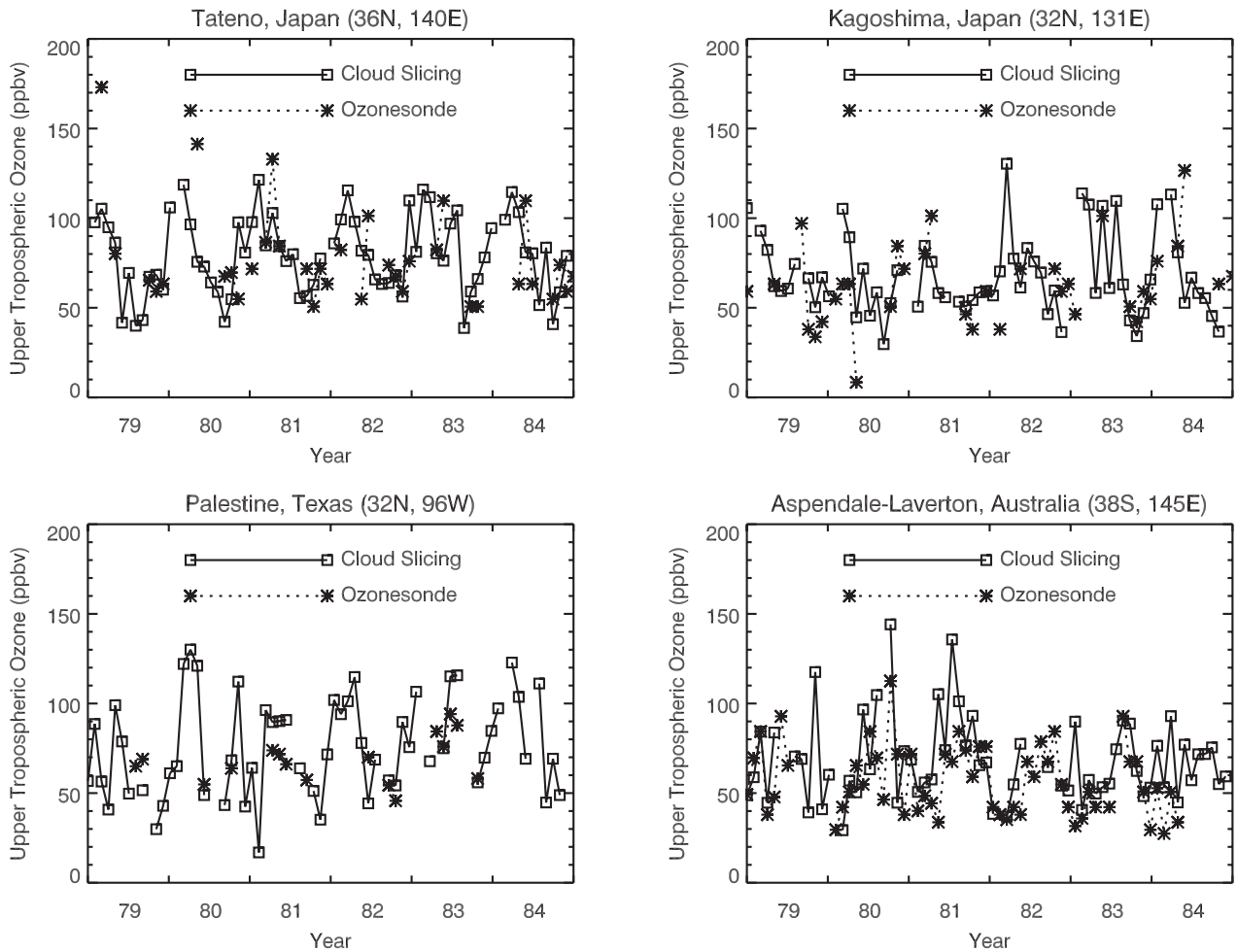

Figure 3a. Monthly ensemble time series (units ppbv) for years 1979–1984 at several WOUDC ground station locations comparing upper tropospheric ozone from cloud slicing with ozonesonde measurements. The four stations shown are Tateno (36°N, 140°E), Kagoshima (32°N, 131°E), Palestine (32°N, 96°W), and Melbourne (38°S,145°E).

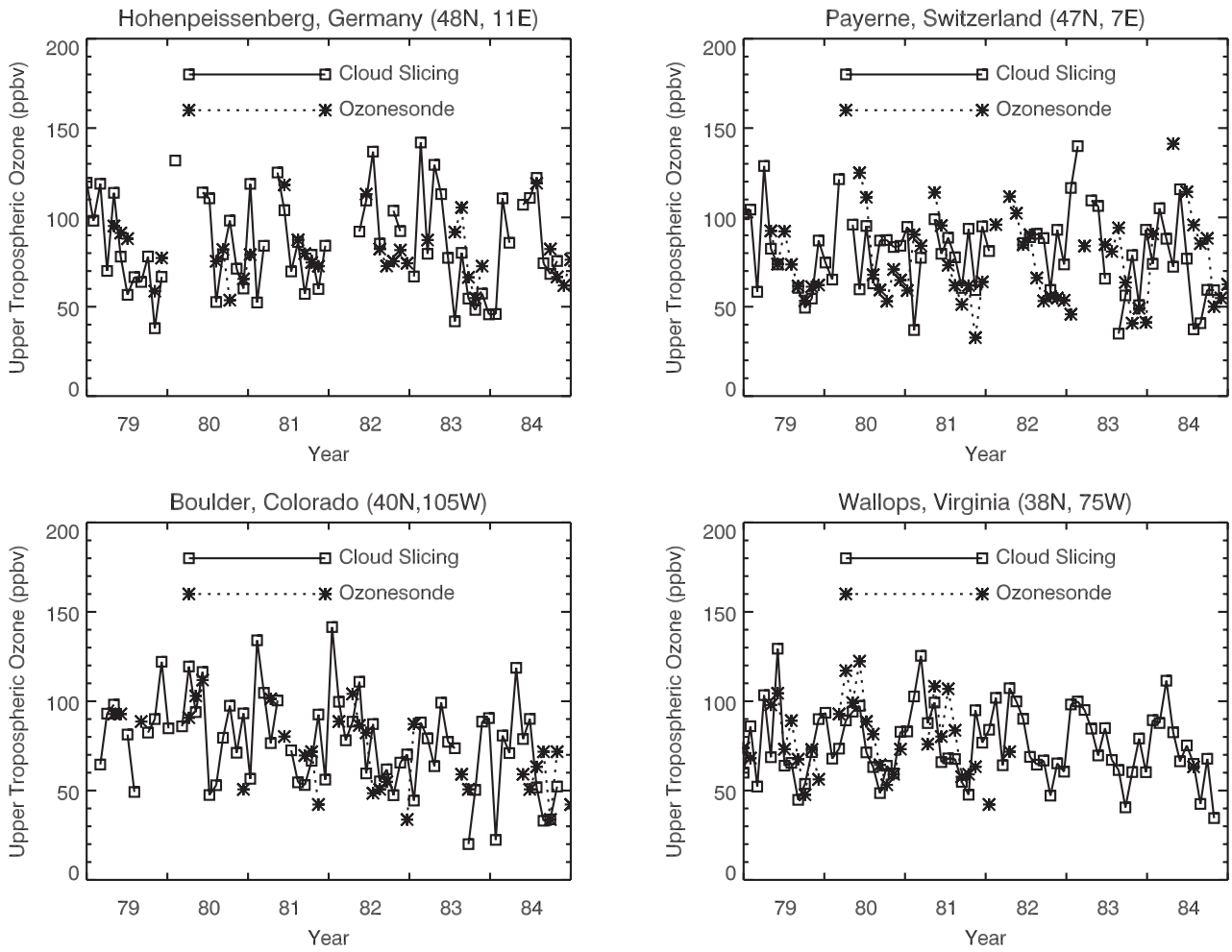

Figure 3b. Same as Figure 3a but for stations Hohenpeissenberg (48°N, 11°E), Payerne (47°N, 7°E), Boulder (40°N, 105°W), and Wallops (38°N, 75°W).

future Earth Observing System (EOS) Ozone Monitoring Instrument (OMI) will reduce this difficulty of measuring special cases. Even better platforms for cloud slicing in the future may be geostationary satellites that could replace the large 100 km diameter footprint measurements from Nimbus 7 with a field-of-view (FOV) down to 0.25 km given current instrument technology (J. R. Herman, personal communication, 2003).

[16] Figures 3a and 3b shows time series comparisons of upper tropospheric ozone at several ground station locations. It is noted that both data sources were constructed as monthly ensembles which do not represent true monthly means. This is because measurements for both sources are scarce with some monthly ensembles having as little as only one day of measurements. Despite data sampling problems, upper tropospheric ozone time series in Figures 3a and 3b indicate general agreement in mean amounts and seasonal variability with greatest abundance around spring months and minimum amounts in autumn in both hemispheres. Figure 4 shows seasonal cycle comparisons of the data plotted in Figures 3a and 3b, including comparisons at several additional ground-station locations. The station locations in Figure 4 begin in the upper leftmost frame for Goose, Canada (53°N, 60°W) and progress with decreasing latitude from left to right and downward by row. Most of the stations are in the NH extratropics (i.e., Europe, Japan, United States) and show largest seasonal variations and mean column amounts in middle to high latitudes. The SH stations (last two frames) show a reversal of the seasonal cycle variability with largest ozone around SH spring months.

[17] Tables 3 and 4 show the average number of monthly measurements used to calculate the seasonal means in Figure 4 for prefiltered ozonesondes (Table 3) and cloud slicing (Table 4). Table 3 indicates that the prefiltering of tropopause pressure less than 200 hPa significantly reduces sonde measurements in winter for stations outside the tropics. *Logan* [1999, Figure 5] shows median tropopause pressure seasonal cycles from low to high latitudes from sonde data. In the low latitudes extending from Samoa (14°S, 170°W) northward to Naha (26°N, 128°E), her analyses shows values of around 100 hPa year-round. In subtropical and higher latitudes her analyses shows significant seasonal variability, particularly for the Japanese stations Tateno (36°N, 140°E) and Sapporo (43°N, 141°E) which both show tropopause pressures of around 100–150 hPa in summer-autumn (July–September) and around 300 hPa in winter (December–February). The point made from Table 3 is that even in winter and spring months outside the tropics it is possible for

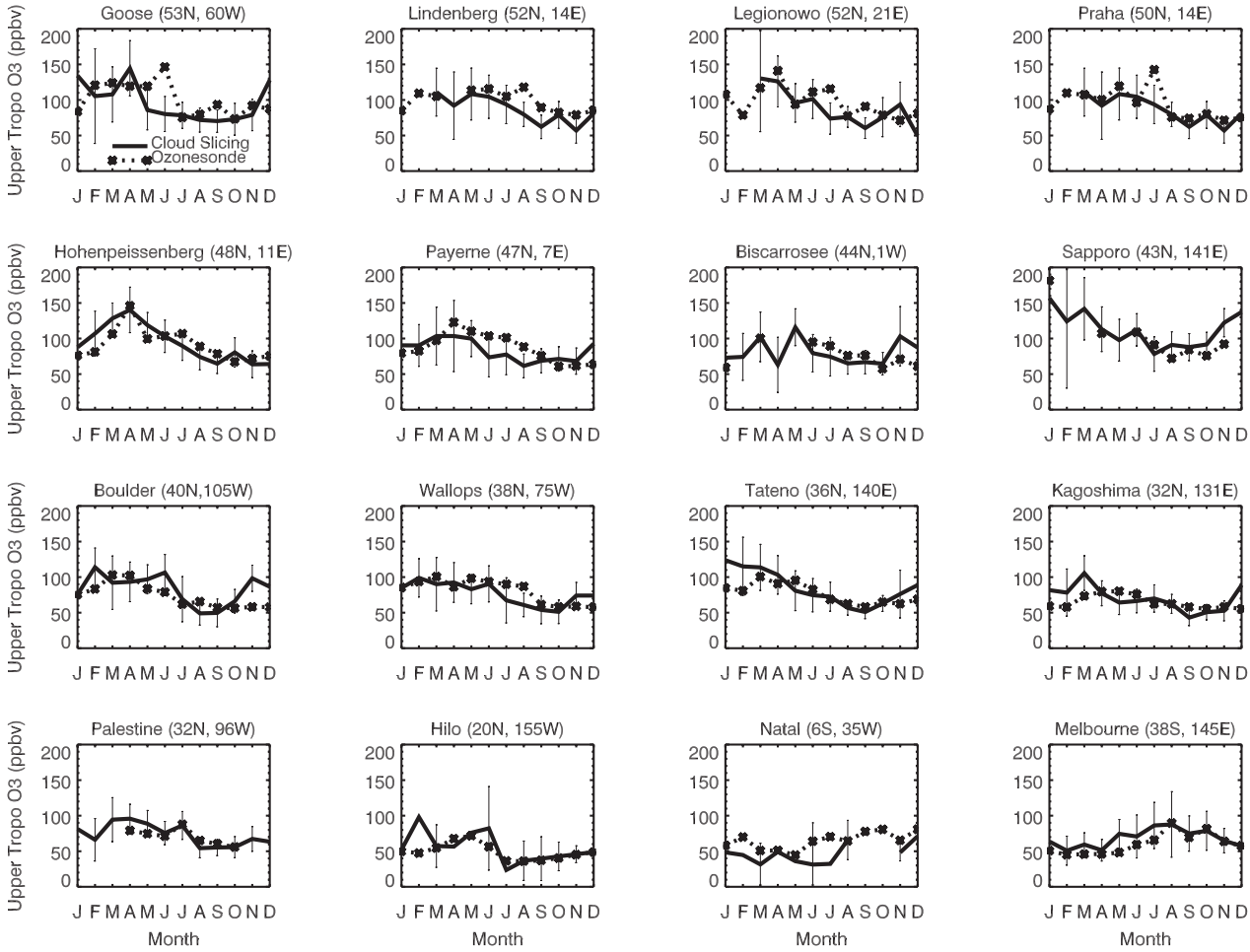

Figure 4. Estimated seasonal cycles of monthly ensemble time series of upper tropospheric ozone volume mixing ratio (units ppbv) from several ground station locations (including stations plotted in Figure 3). Years used in averaging: 1979–1984 (cloud slicing); 1979–1998 (sonde). Cloud slicing measurements are solid lines; ozonesonde measurements are dashed lines. Cloud slicing measurements include $\pm 2\sigma$ statistical uncertainties.

low tropopause pressure conditions to exist and are likely caused by intense episodic baroclinic disturbances.

[18] There have been many studies of ozone in the 200–500 hPa pressure range from instruments onboard aircraft. A few of these instrument platforms include various Global Tropospheric Experiment (GTE) missions (web page http://www-gte.larc.nasa.gov/), Nitrogen Oxides and Ozone along Air Routes (NOXAR) [e.g., *Brunner et al.*, 2001, and references therein], Subsonic assessment, Ozone and Nitrogen oxide Experiment (SONEX) [e.g., *Liu et al.*, 1999, and

Table 3. Number of Months During 1979–1998 Having Sonde Measurements With Cold-Point Tropopause Pressure Less Than 200 hPa

Station	Jan.	Feb.	March	April	May	June	July	Aug.	Sept.	Oct.	Nov.	Dec.
Goose (53°N, 60°W)	1	2	1	3	4	4	2	3	5	4	2	1
Lindenberg (52°N, 14°E)	9	2	3	0	3	7	4	6	10	13	10	8
Legionowo (52°N, 21°E)	5	5	1	4	1	5	1	2	13	12	6	8
Praha (50°N, 14°E)	9	6	2	3	3	2	2	2	2	2	2	2
Hohenpeissenberg (48°N, 11°E)	6	3	4	2	4	6	10	14	17	15	13	14
Payerne (47°N, 7°E)	9	4	3	4	7	10	15	14	15	15	13	13
Biscarrosse (44°N, °W)	3	0	1	0	0	4	2	4	3	2	4	4
Sapporo (43°N 141°E)	1	0	0	3	8	7	7	7	11	9	4	0
Boulder (40°N 105°W)	5	3	2	12	13	16	11	13	16	11	8	8
Wallops (38°N, 75°W)	6	6	3	8	13	11	16	14	13	13	15	12
Tateno (36°N 140°E)	9	5	6	13	18	11	7	7	17	18	17	14
Kagoshima (32°N 131°E)	14	10	10	13	16	9	7	7	11	16	16	18
Palestine (32°N 96°W)	0	0	0	2	3	5	1	1	3	3	0	0
Hilo (20°N 155°W)	14	13	12	12	12	13	13	13	14	14	13	15
Natal (6°S, 35°W)	4	3	4	5	4	3	4	5	5	5	4	3
Laverton (38°S 145°E)	10	13	10	9	8	4	3	4	3	4	6	11

Table 4. Number of Months During 1979–1984 Included in 6-Year Means for Cloud Slicing

Station	Jan.	Feb.	March	April	May	June	July	Aug.	Sept.	Oct.	Nov.	Dec.
Goose (53°N, 60°W)	3	4	5	5	5	6	6	6	6	6	5	4
Lindenberg (52°N, 14°E)	1	0	5	2	4	4	4	6	5	6	4	1
Legionowo (52°N, 21°E)	2	0	2	2	5	4	4	6	4	4	4	1
Praha (50°N, 14°E)	1	0	5	2	4	4	4	6	5	6	4	1
Hohenpeissenberg (48°N, 11°E)	4	5	5	4	5	6	6	6	5	6	5	4
Payerne (47°N, 7°E)	6	5	5	3	5	6	4	5	6	6	5	5
Biscarrosse (44°N, 1°W)	4	2	4	3	5	4	3	3	5	5	3	5
Sapporo (43°N 141°E)	2	2	4	5	6	6	5	5	6	6	5	4
Boulder (40°N 105°W)	5	5	6	6	6	5	6	5	5	6	5	5
Wallops (38°N, 75°W)	6	6	6	6	6	6	6	6	6	6	5	5
Tateno (36°N 140°E)	6	5	6	6	6	6	6	6	6	6	6	4
Kagoshima (32°N 131°E)	4	3	6	6	6	6	5	6	5	6	5	4
Palestine (32°N 96°W)	6	4	6	5	6	5	4	2	4	5	5	5
Hilo (20°N 155°W)	5	4	3	2	2	2	1	4	1	4	4	4
Natal (6°S, 35°W)	3	4	3	3	3	2	1	1	0	0	3	3
Laverton (38°S 145°E)	6	4	6	6	6	4	4	5	5	v5	6	5

references therein], and Measurement of Ozone and Water Vapor by Airbus In-Service Aircraft (MOZAIC) [e.g., *Marenco et al.*, 1998]. Comparisons of Nimbus 7 cloud slicing data with these aircraft measurements is difficult for two important reasons: (1) ozone measurements from cloud slicing always lie below the tropopause and (2) cloud slicing measurements coincide with dynamically-intense convection events over large geographical regions. Aircraft flight paths at cruising altitude often encounter some amount of stratospheric air mass and ozone, especially in middle to high latitudes. This violates condition (1). Also, the aircraft usually fly around intense convective regions like the ones required for Nimbus 7 cloud slicing, and this violates condition (2).

[19] Our best comparison with cloud slicing comes from the ozonesonde data which, if in situ temperature profiles were made, can be filtered for various states of tropopause height conditions. *Logan* [1999, Figures 8 and 13] shows ozonesonde mixing ratio median seasonal cycles at the tropopause, 2 km above the tropopause, and 1 km below the tropopause. At 2 km above the tropopause there is, especially for the higher latitudes, a tendency for a distinct springtime maximum. At the tropopause and 1 km below, the seasonal maximum shifts more toward summer months. In our study we prefiltered all ozonesonde data for a tropopause pressure (cold-point definition) less than 200 hPa prior to comparing with cloud slicing data. In winter-spring months in the sonde data there is a tendency for some amount of high ozone present below the cold-point tropopause. In comparison, the cloud slicing measurements, which are always ozone measurements below the tropopause, also show largest amounts in winter and spring. After comparing the prefiltered ozonesonde data with the cloud slicing measurements, we cannot rule out possible stratospheric ozone influence given the intense dynamical convective events associated with cloud slicing, particularly during winter and spring months in the extratropics when lower-stratospheric ozone is largest.

4. Characterization of Seasonal Cycles and Spatial Distributions

[20] The main purpose of this study is to investigate the feasibility of extending cloud slicing to middle and high latitudes and to characterize observed seasonal cycles and spatial distributions of derived upper tropospheric ozone. Figure 5 shows spatial distributions of 6-year averaged 3-month seasonal means (indicated) of upper tropospheric ozone volume mixing ratio. Largest ozone occurs in winter and spring months in both hemispheres with greater abundance in the NH. The most significant amounts occur in middle to high latitudes. In the NH midlatitudes in winter and spring months there is evidence of partial poleward entrapment of upper tropospheric ozone caused by the upper tropospheric wind jets which can act as a partial barrier for meridional transport of air mass in the upper troposphere. In the NH in winter and spring there are large meridional gradients and enhancements in ozone along wind-driven storm track regions such as the eastern United States and the Asian continent extending into the eastern Pacific. In the SH in winter and spring seasons the horizontal gradients and mean amounts in ozone are weaker than winter and spring seasons in the NH. There is also a persistent feature present in each season in the SH subtropics which indicates an enhancement of ozone near South America, Africa, and Australia. In the tropics, enhancement of upper tropospheric ozone is present each season in the Atlantic region from South America to Africa compared to the eastern and western Pacific regions.

[21] The seasonal and spatial characteristics of upper tropospheric ozone in Figure 5 resemble that of total column ozone (Figure 6). We note that the near-global similarity of upper tropospheric ozone and total ozone is not an artifact of the cloud slicing algorithm. The algorithm assumes that stratospheric column ozone is spatially invariant over each selected $5^\circ \times 5^\circ$ region. That is, all above-cloud column ozone variability over the region is tropospheric in origin. This requirement is not generally satisfied within tropospheric wind jet regions where the tropopause height changes dramatically. These regions are limited mostly to narrow meandering bands in the subtropics and middle latitudes. The cloud slicing algorithm removes outlier data associated with these wind jet regions by applying statistical and total column ozone filtering (see Appendix A).

[22] The most robust spatial similarities between upper tropospheric ozone in Figure 5 and total ozone in Figure 6 occur in the NH in winter and spring months. Because

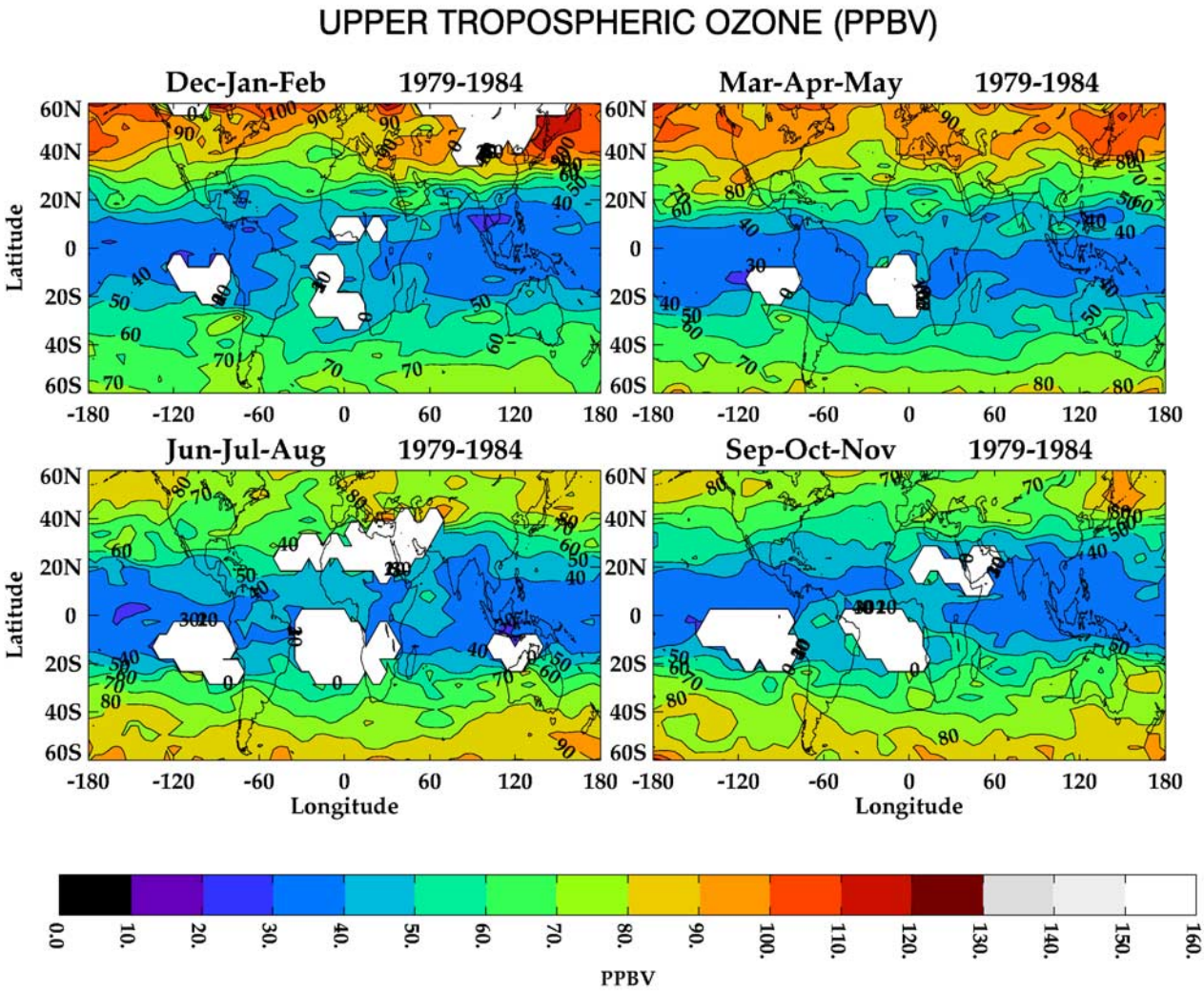

Figure 5. Seasonal averages (DJF, MAM, JJA, SON, indicated in each frame) of TOMS upper tropospheric ozone volume mixing ratio (units ppbv) between 60°S and 60°N derived from cloud slicing. Seasonal averages incorporated 1979–1984 Nimbus 7 TOMS/THIR colocated measurements of above-cloud column ozone and cloud-top pressure.

ozone is generally a long-lived tracer of air mass in both the upper troposphere and lower stratosphere (lifetimes of months to years, respectively), the patterns in Figures 5 and 6 suggest a possible influence from STE (discussed in section 5). Figures 7 and 8 show zonal mean seasonal cycles from the data plotted in Figures 5 and 6. It is noted for the upper tropospheric ozone data in Figure 7 that these are not true zonal means since in several months there are regions without enough clouds for applying the cloud slicing method (e.g., see Figure 5 and discussion). Nevertheless, in Figures 7 and 8 both upper tropospheric ozone and total column ozone show similar seasonal variation and latitude dependence. In the tropics seasonal cycles are different in these quantities, and both temporal and meridional variations appear weak. Outside the tropics, mean amounts and meridional gradients are greatest around spring months in both hemispheres.

[23] Figure 9 shows zonal mean upper tropospheric ozone for January 1979-October 1984. As in Figure 7, variabilities in upper tropospheric ozone in Figure 9 show largest latitudinal gradients in the extratropics of both hemispheres with peak amounts around spring months. It is noted that the springtime maximum in upper tropospheric ozone volume mixing ratio in NH middle and high latitudes agrees with the NH ozonesonde climatology assessment of *Logan* [1999] (e.g., Logan's Figure 27 for 300 hPa in middle to high latitudes and 200 hPa in the subtropics). Figure 9 indicates a possible semiannual component in the tropics. Peak-to-peak amplitudes of this signal are weak, around 2–4 ppmv. In some years (e.g., 1980–1983) there is evidence of a semiannual oscillation while in other years there is not. A semiannual component in the tropics may indicate a dynamical and/or photochemical forcing related to the semiannual zenith crossing of the sun in the tropics. Comparisons of the semiannual and annual variations in total column ozone and upper tropospheric ozone are shown in Figure 10. The annual and semiannual amplitudes were derived by applying basic Fourier analysis. Both annual and semiannual components in total ozone and upper tropospheric ozone in Figure 10 compare well in a global sense

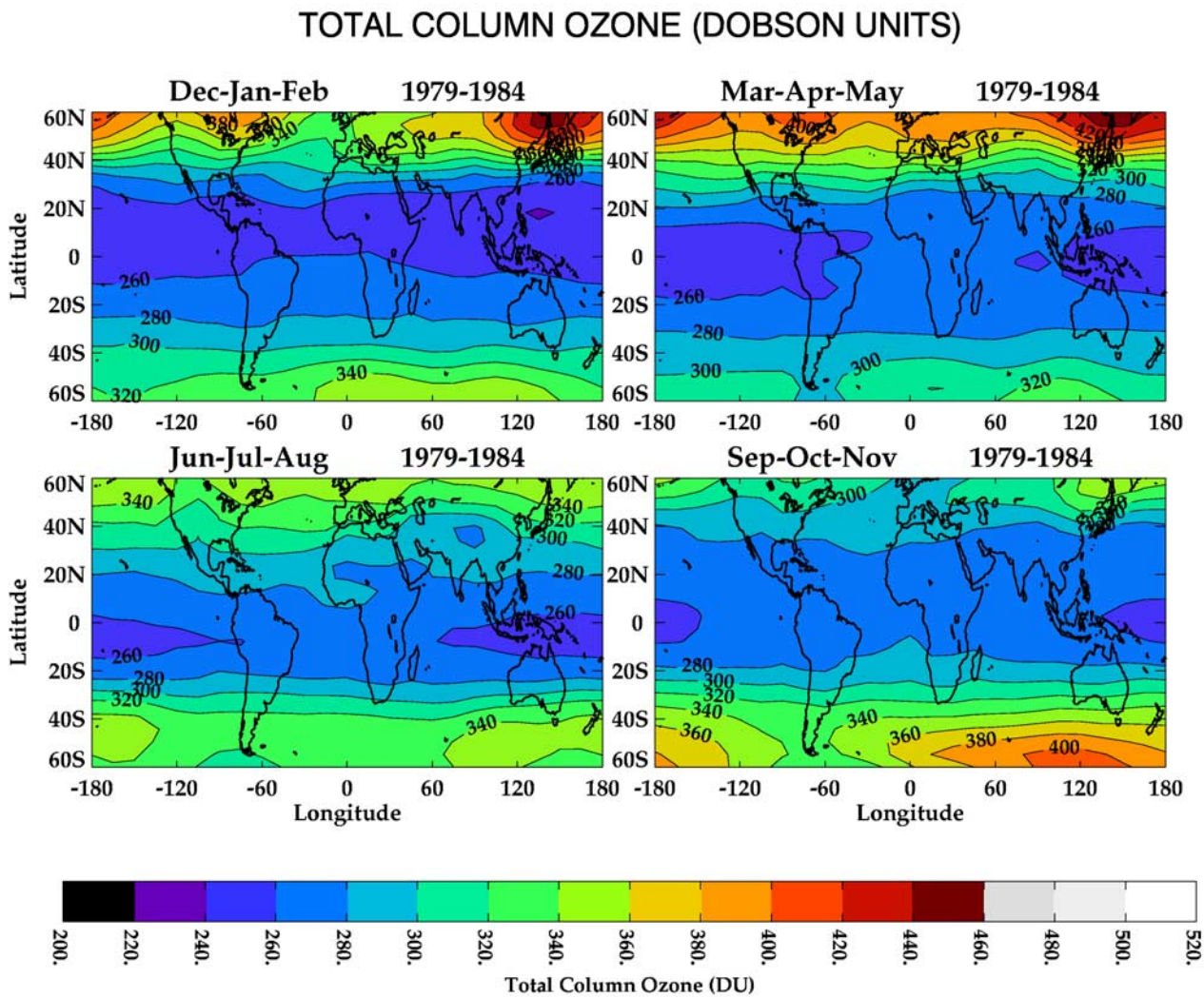

Figure 6. Same as Figure 5 but for TOMS total column ozone (in Dobson units).

with annual cycle variations exhibiting larger amplitudes and larger latitudinal gradients.

5. Correlations of Seasonal Cycles

[24] It has been shown that total ozone and upper tropospheric ozone from cloud slicing indicate similar spatial and seasonal cycle variabilities extending from low to high latitudes. A possible explanation for these coherent temporal and spatial relationships may be STE processes in the atmosphere that occur under conditions of intense broad-scale convective events associated with Nimbus 7 cloud slicing scenes. Ozone in the upper troposphere and lower stratosphere is a relatively long-lived chemical tracer (e-folding lifetimes of months to years, respectively) so that even monthly measurements in this study provide valuable insight regarding possible occurrence of STE. Recent studies suggest that tropopause folding and turbulent convection are significant sources for transporting stratospheric air mass into the troposphere [e.g., *Langford et al.*, 1996; *Beekmann et al.*, 1997; *Cho et al.*, 1999; *Eisele et al.*, 1999; *Meloen et al.*, 2001; *Bertin et al.*, 2001; *Fujiwara and Takahashi*, 2001]. The global effects of STE on tropospheric ozone and its seasonal variability may be significant. The 3D model study by *Lelieveld and Dentener* [2000] indicated that upward of 80% of tropospheric ozone may be ascribed to STE in subtropical-to-high latitudes. We note however that the 3D model by *Wang et al.* [1998] suggested significantly smaller contribution from STE at around 10% when averaged either over a hemisphere or globally (Wang et al.'s Table 1).

[25] *Appenzeller et al.* [1996, and references therein] showed that air mass lying in the lowermost stratosphere is fundamental to global STE processes. This study investigates potential STE on observed upper tropospheric ozone seasonal cycles by comparing with both lower stratospheric ozone and lower stratospheric air mass. Air mass abundance in the lowermost stratosphere is parameterized from tropopause pressure (see Appendix B). For lower stratospheric ozone we include measurements from the UARS HALOE instrument. HALOE is a solar occultation instrument which provides profile information of stratospheric ozone from the top of the atmosphere down to the tropopause [*Bruhl et al.*, 1996]. Mean ozone volume mixing ratio from HALOE was

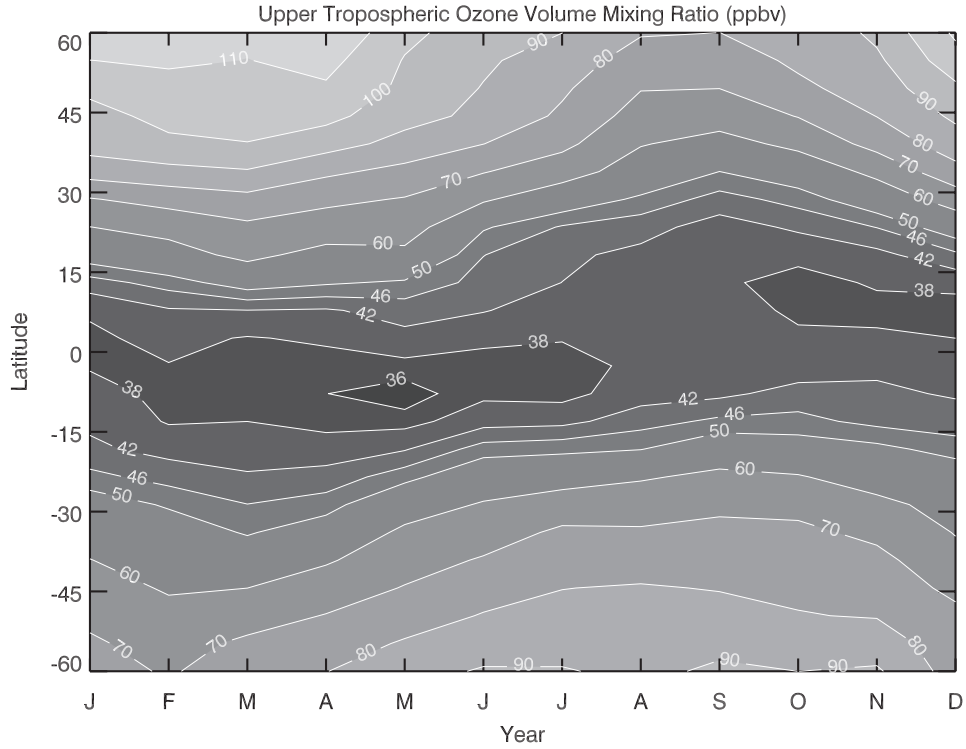

Figure 7. Latitude versus month zonally averaged seasonal cycles in upper tropospheric ozone volume mixing ratio (units ppbv) from cloud slicing. Seasonal cycles were derived from TOMS and THIR colocated measurements for 1979–1984.

calculated for both the 46–100 hPa and 46–215 hPa pressure bands (i.e., together encompassing the lower stratosphere extending from tropics to high latitudes) for the 1993–2000 post-Pinatubo time period. Although for a time period later than 1979–1984 and with sparse temporal and spatial coverage as an occultation instrument, the combined 8 years of HALOE measurements provide retrievals of lower stratospheric column ozone adequate to

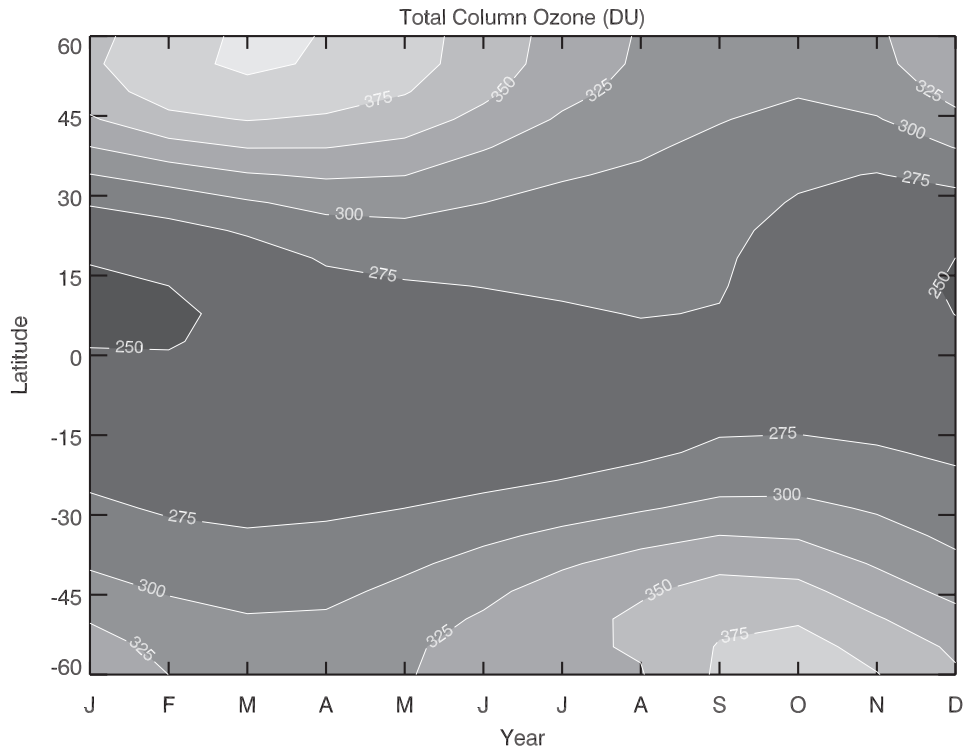

Figure 8. Similar to Figure 7 but for TOMS total column ozone in Dobson units.

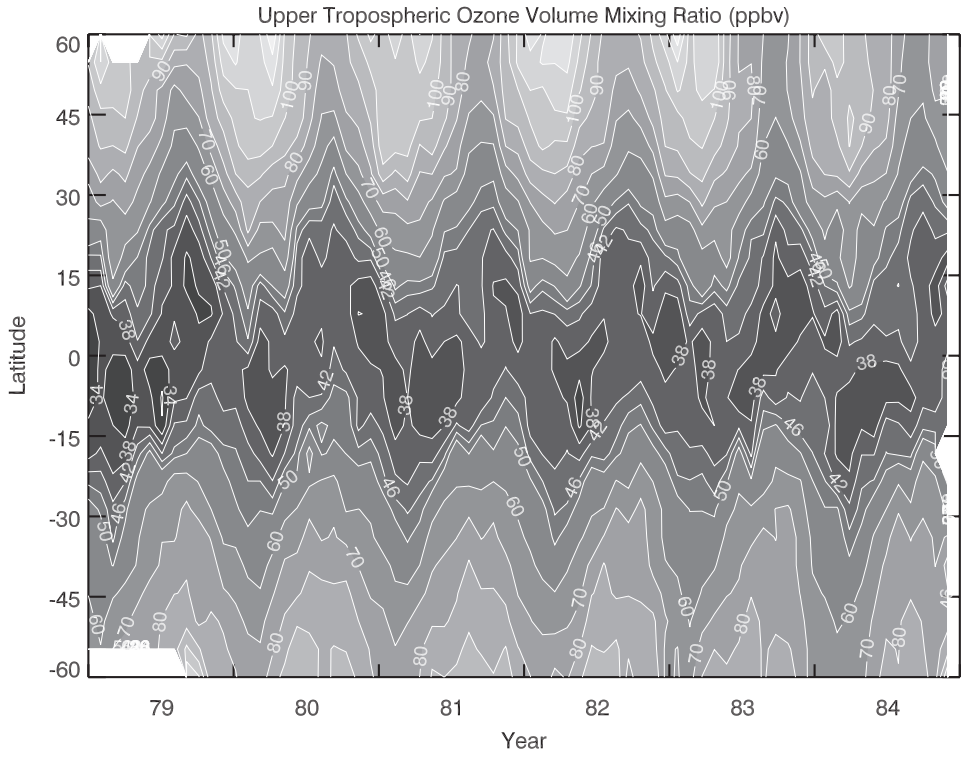

Figure 9. Upper tropospheric zonal mean ozone volume mixing ratio for January 1979 to December 1984. Units are ppbv.

develop seasonal cycles for this comparison. Figure 11 shows seasonal cycles in HALOE zonal mean ozone volume mixing ratio for the 46–100 hPa pressure band evaluated for 1993–2000. For latitudes less than around 25°–30° the 46–100 hPa pressure band represents the lower stratosphere. At higher latitudes the pressure band is more representative of the middle to lower stratosphere. Seasonal variabilities of HALOE ozone in Figure 11 are comparable to seasonal variabilities in upper tropospheric ozone in middle to high latitudes (compare Figure 11 with Figure 7).

[26] Figure 12 shows temporal correlations as a function of latitude between upper tropospheric ozone and HALOE (stars, long-dashed curves), TOMS total column ozone (bold), and NCEP tropopause pressure (dotted). Correlation calculations with 46–215 hPa HALOE measurements were not plotted in Figure 12 equatorward of 35° latitude because 215 hPa exceeds tropopause pressure in these lower latitudes in winter and spring months. The correlations in Figure 12 are based on 12 months of zonal mean data at each latitude and therefore prescribe only basic agreement or disagreement between seasonal cycles. Correlation

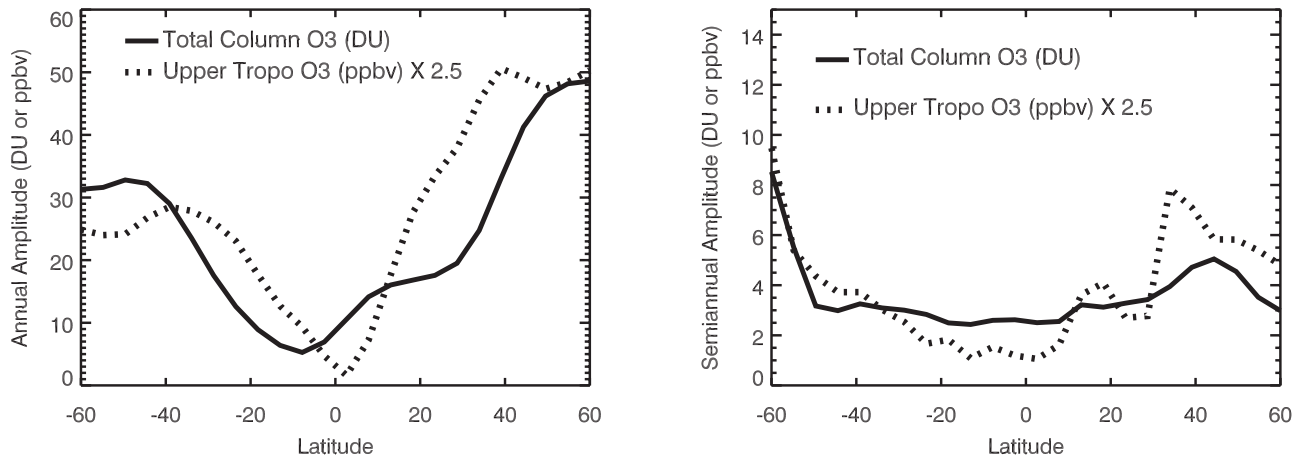

Figure 10. Comparisons of the annual (left) and semiannual (right) amplitudes in total column ozone (solid line) and upper tropospheric ozone (dashed line). Annual and semiannual amplitudes were derived by applying basic Fourier analysis to the 1979–1984 monthly ensemble time series data. Units for both annual and semiannual amplitudes are ppbv.

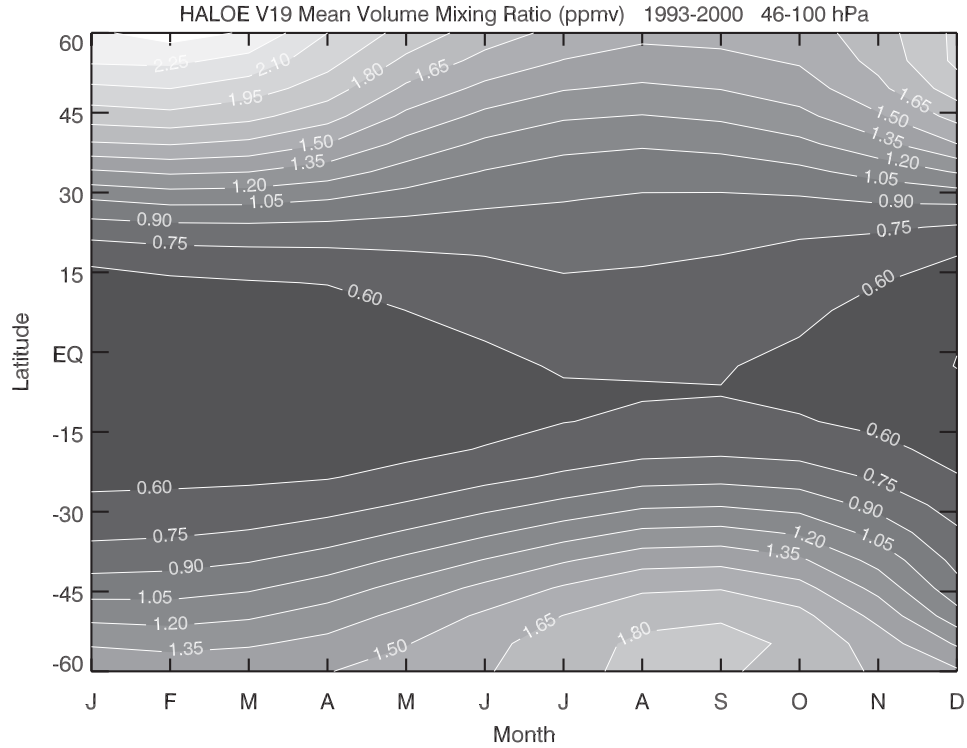

Figure 11. Latitude versus month zonally averaged seasonal cycles in lower stratospheric (46–100 hPa) mean ozone volume mixing ratio (units ppmv) from HALOE measurements.

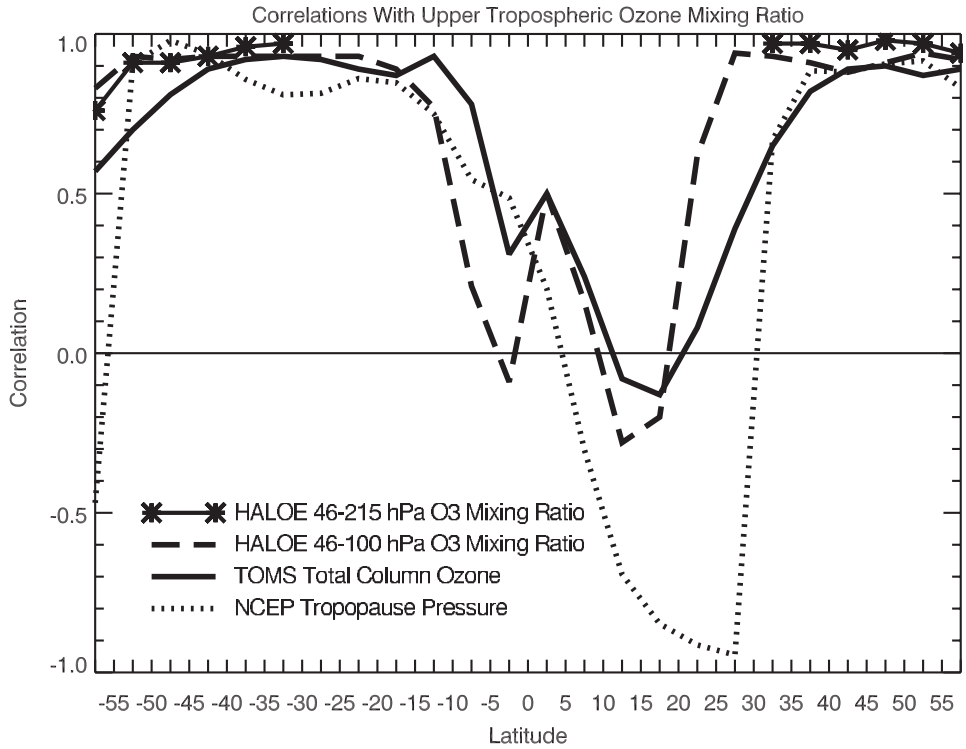

Figure 12. Latitude-dependent temporal correlations between upper tropospheric ozone and HALOE (long-dashed line, stars), TOMS total column ozone (thick solid line), and NCEP tropopause pressure (short-dashed line). Correlation amplitudes exceeding 0.58 pass 95% confidence level (i.e., 5% significance level). Seasonal cycles for upper tropospheric ozone, total ozone, and NCEP tropopause pressure were determined from 1979–1984 data. Seasonal cycles for HALOE lower stratospheric column ozone were evaluated for the 1993–2000 (i.e., post-Pinatubo) time period.

amplitudes exceeding 0.58 pass 95% confidence level (i.e., 5% significance level). Seasonal cycles for upper tropospheric ozone, total ozone, and NCEP tropopause pressure were determined from 1979–1984 data. Seasonal cycles for HALOE lower stratospheric column ozone were evaluated for the 1993–2000 (i.e., post-Pinatubo) time period. We note that the 200 hPa and 500 hPa lower and upper pressure boundaries chosen for cloud slicing (discussed in section 2) are not representative of the same part of the troposphere at all latitudes. In middle and high latitudes the measurements are clearly upper troposphere. In the tropics they are middle to upper troposphere.

[27] If STE is the dominant source of ozone seasonal variability in the upper troposphere for the cloud slicing events, then all four curves in Figure 12 would conceivably have correlations near +1 at latitudes where this persists. In subtropical-to-high latitudes, NCEP tropopause pressure and both HALOE lower stratospheric ozone and TOMS total ozone measurements all indeed show correlations near +1. However this is not the case in the low latitudes in Figure 12 extending from around 10S to 25N. In these lower latitudes the correlations with NCEP tropopause pressure become negative in the NH tropics and correlations with HALOE and TOMS are greatly reduced to low-to-negative values. The poorest correlations occur in the NH tropics and are caused by a seasonal maximum in upper tropospheric ozone during NH spring season compared to seasonal maxima around NH autumn months in NCEP tropopause pressure, TOMS total ozone, and HALOE lower stratospheric ozone (note seasonal cycle differences for mean ozone volume mixing ratio in Figures 7 and 11 in the NH tropics). We note that a springtime maximum in the tropical northern latitudes was also present in the 100–400 hPa cloud slicing analyses by *Ziemke et al.* [2001], similar to the 200–500 hPa analyses in this study. (The 100–400 hPa analyses are more representative of upper tropospheric ozone in the tropics.) Several potential sources of upper tropospheric ozone could explain the seasonal cycles for latitudes 10S to 25N including biomass burning, biogenic emissions, aerosol influenced photochemistry, tropospheric transport, and cloud lightning [e.g., *Moxim and Levy*, 2000; *Lelieveld and Dentener*, 2000; *Bey et al.*, 2001; *Martin et al.*, 2001, 2002].

6. Summary

[28] This study has examined the spatial distributions and seasonal cycles in upper tropospheric ozone (pressure range 200–500 hPa) between 60°S to 60°N from "cloud slicing". Previous investigations have had limited success in measuring tropospheric ozone beyond tropical latitudes from satellite data. cloud slicing is a method for determining ozone profile information in the troposphere by combining colocated measurements of cloud-top pressure and above-cloud column ozone. Because the method uses tropospheric clouds, the ozone measured always lies below the tropopause. Given the large FOV (~100 km diameter footprints on average) from Nimbus 7 TOMS, upper tropospheric ozone measured from this method corresponds to generally sparse highly dynamical convection events over broad regions. The behavior of upper tropospheric ozone during these events is not necessarily representative of typical conditions in the atmosphere, especially poleward of the tropospheric wind jets (around ± 30 degrees of latitude), and particularly in winter and spring when episodic dynamical wave activity in the troposphere and lower stratosphere vary significantly.

[29] Comparisons were made between upper tropospheric ozone volume mixing ratio derived from cloud slicing and ground-based ozonesondes for 60°S to 60°N. The best agreement between the two data sources occurred when the ozonesonde data were prefiltered for low tropopause pressure (less than 200 hPa). Low tropopause pressure in the extratropics coincides with the passage of baroclinic disturbances and convection. The ozonesonde and cloud slicing data compared favorably in monthly ensemble time series and seasonal cycles despite sparse measurements available from either data source. These comparisons indicate the efficacy of this method even as applied to the relatively coarse FOV scanning measurements from Nimbus 7 TOMS. Future satellite instruments with smaller footprint size and greater spectral resolution than TOMS may provide significant improvements to the cloud slicing method, with larger number of measurements and application to constituents other than ozone.

[30] Upper tropospheric ozone indicates a possible semiannual component variability in the tropics. A semiannual oscillation appears in some years but not in other years which may be a result of poor signal-to-noise with the Nimbus 7 measurements. The existence of a semiannual component in the tropics may indicate a dynamical and/or photochemical forcing related to the twice per year zenith crossing of the sun in tropical latitudes.

[31] Ozone measurements from Nimbus 7 cloud slicing coincide with large-scale dynamically-intense convection. Associated with such broad-scale convection is a turbulent atmosphere with the potential for stratospheric ozone transport into the upper troposphere (either reversibly or irreversibly), most notably in regions near and poleward of the tropospheric wind jets (around ±30° latitude). Our analyses indicate that spatial patterns in upper tropospheric ozone were found to be similar to total column ozone, particularly in the NH during winter-spring. Given long lifetimes (months to years, respectively) for ozone in the upper troposphere and lower stratosphere, ozone in these regions of the atmosphere is a tracer of air mass movement and distribution. The spatial patterns and seasonal cycles in middle to high latitudes in both hemispheres are similar for TOMS total ozone, lower stratospheric ozone from UARS HALOE, NCEP lower stratospheric air mass, and upper tropospheric ozone from TOMS cloud slicing. The mean amounts and seasonal variabilities in upper tropospheric ozone in the extratropics are both larger in the NH compared to the SH. These observations along with previous 2D and 3D model results indicate possible occurrence of STE in the extratropics.

[32] Comparisons between lower stratospheric air mass, stratospheric ozone, and upper tropospheric ozone imply that STE does not appear to be a major source for the seasonal variability of ozone in the upper troposphere in low tropical latitudes extending over a broad region from around 10°S to 25°N. In these latitudes there is poor temporal correlations in seasonal cycles between troposphere and stratosphere, especially in NH tropical latitudes were largest

amounts of upper tropospheric ozone from cloud slicing occur in spring months. There are several sources for upper tropospheric ozone that could explain the seasonal cycles in low latitudes. These sources include biomass burning, biogenic emissions, aerosol influenced photochemistry, tropospheric transport, cloud lightning, etc. (beyond the extent of this study).

Appendix A: Cloud Slicing Algorithm

[33] Cloud slicing was applied to daily ensemble measurements over 5° × 5° binned regions, and then averaged within each month for the January 1979–October 1984 time period. The chosen latitude coverage of colocated TOMS and THIR footprint measurements extends from 60°S to 60°N. This reduces difficulties of persistent snow and ice in the polar regions and also eliminates problems with polar night conditions where there are no TOMS backscattered UV ozone measurements. For the cloud slicing technique, footprint measurements (50 km × 50 km at Nadir, around 100 km × 100 km on average) of above-cloud column ozone from Nimbus 7 TOMS are plotted versus colocated measurements of Nimbus 7 THIR cloud-top pressure over a preselected pressure band (200–500 hPa in this study). The mean slope of the distribution then directly yields mean volume mixing ratio for ozone within that pressure band. Specifically, mean volume mixing ratio (X, in ppmv) is determined from [e.g., *Ziemke et al.*, 2001, and references therein]

$$X = 1.27\ \Delta\Omega/\Delta P, \tag{A1}$$

where Ω is above-cloud column ozone (in DU), and P is cloud-top pressure (in hPa). *Eck et al.* [1987] showed for Nimbus 7 TOMS that footprint scenes with reflectivity greater than 0.4 are almost always 100% cloud-filled (i.e., 100% cloud fraction scenes). Only scenes with reflectivity greater than 0.44 were selected in this study to eliminate most partially cloudy footprint scenes. This reflectivity filtering is a relaxation from the more stringent 0.6 value of reflectivity used by *Ziemke et al.* [2001] and provides a greater proportion of scenes for applying cloud slicing. Another important parameter is the minimum number of daily colocated measurements of ozone and cloud pressure within each 5° × 5° region. This number was selected (for adequate statistics) in the present study to be at least 20, and as in the work of *Ziemke et al.* [2001], only computed mixing ratio values greater than the statistical 2σ value were retained.

[34] We note that with optically thick clouds, some of the column ozone detected from TOMS is ozone lying inside the cloud's upper level. The cause is multiple scattering of ozone inside the cloud tops. The multiple scattering produces additional absorption of backscattered UV photons which produces an over-determination (several DU) of above-cloud column ozone (Z. Ahmad and M. Newchurch, personal communication, 2003). While this does affect above-cloud column measurements, it will not significantly affect cloud slicing measurements (derived ozone is the mean slope of ozone versus pressure) if actual upper tropospheric ozone inside the clouds is homogeneous over the region used for cloud slicing.

[35] A fundamental assumption with cloud slicing is that stratospheric column ozone is invariant over the selected region (i.e., all above-cloud column ozone changes over the region are tropospheric in origin). This condition breaks down in and near strong dynamical regions, particularly the tropospheric wind jet regions where stratospheric column ozone may exhibit large zonal and meridional variability. An additional filter is applied to identify these regions: Following analysis for each daily 5° × 5° gridded region, only horizontal gradients in above-cloud column ozone ($|\Delta\Omega|$) less than 50 DU were retained in the data base. This number was chosen subjectively following several trial runs with Nimbus 7 cloud slicing. It is likely that there is some stratospheric contamination in the retrievals, but these effects are expected to be limited mostly to narrow regions associated with the tropospheric wind jets. The consistency with ozonesonde measurements (section 3) and lack of obvious outliers in these regions suggest that the algorithm does not produce a significant amount of stratospheric ozone gradient contamination in the retrievals. It is noted that it is also possible to identify the wind jet regions using global meteorological analyses such as from NCEP, but there are two reservations for doing this given the type of measurements associated with cloud slicing: (1) The analyses have a coarse resolution compared to the size of TOMS footprint measurements, and (2) the analyses must be accurate to within about 100 km to 200 km in identifying the location of the wind jets, otherwise a significant portion of bad data may be retained and good data dispensed with cloud slicing.

Appendix B: Column Abundance and Air Mass in the Atmosphere

[36] One can relate ozone and air mass in the atmosphere in a self-consistent way using the concept of column abundance and the Dobson Unit. The fundamental Dobson Unit definition applies to all constituents in the atmosphere, including the total atmosphere itself where both volume and mass mixing ratio are unitary (100 percent content). One Dobson Unit (DU) is equivalent to 10^{-5} m vertical thickness of constituent under conditions of standard pressure (1013.25 hPa) and standard temperature (273.16K) [e.g., *Andrews et al.*, 1987, and references therein]. Under this definition, column amount (Ω, in DU) between two pressure surfaces P_1 and P_2 may be determined by integrating volume mixing ratio (X, in units ppmv) over pressure P (in units hPa) from

$$\Omega = 0.79 \int_{P_1}^{P_2} X dP \tag{B1}$$

The constant 0.79 in (B1) was derived for upper tropospheric levels [*Ziemke et al.*, 2001], but can be applied to any constituent in the troposphere or stratosphere with at most around 1% relative error. For the total atmosphere, X is a constant (10^6 ppmv) in (B1) which yields a simple relationship for computing the total air column lying between two arbitrary pressure levels P_1 and P_2: $\Omega = 7.9 \times 10^5 (P_2 - P_1)$. For the global mean surface terrain pressure (about 990 hPa

from NCEP reanalyses) this yields a global mean column amount Ω of 7.8×10^8 DU for the total atmosphere.

[37] Mass associated with column amount Ω is determined by integrating local measurements of Ω over surface area element dS (units m^2):

$$M = \sigma \int_S \Omega ds \tag{B2}$$

It is well known that one Dobson Unit is equivalent to 2.69×10^{20} molecules m^{-2} [e.g., *Ziemke et al.*, 2001, and references therein]. This number applies to any individual constituent in the atmosphere including the total atmosphere itself. In (B2), it follows that σ is the surface mass column density (units kg m^{-2} DU^{-1}) and is equivalent to $2.69 \times 10^{20}\mu/N_A$, where μ is mean molecular weight (48 for ozone, around 29 for the total atmosphere) and N_A is Avogadro's constant (6.022×10^{26} particles $kmol^{-1}$). For the total atmosphere of the Earth, the column amount 7.8×10^8 DU from (B1) applied to (B2) yields a total mass of around 5.2×10^{18} kg. In comparison, for ozone in the atmosphere the average total column is about 300 DU and the total mass of ozone is around 3.3×10^{12} kg.

[38] From (B2), a surface mass density associated with local measurements of Ω is given by $\sigma\Omega$. For NCEP atmospheric air mass this parameter becomes $7.9 \times 10^5\sigma(P_2 - P_1)$. It follows that a proxy for lower stratospheric air mass can be obtained by replacing P_2 with tropopause pressure from NCEP reanalyses and choosing P_1 as an arbitrary constant pressure lying above the tropopause. This investigation uses NCEP tropopause pressure as a first-order proxy of lower stratospheric air mass for cross-correlations of seasonal cycles with upper tropospheric ozone volume mixing ratio from cloud slicing (section 5). As final note, we have incorporated NCEP tropopause pressure which was calculated from the cold-point definition (discussed in section 3).

[39] **Acknowledgments.** We wish to thank Zia Ahmad, Joanna Joiner, and Sasha Vasilkov for important discussions on clouds and related retrieval of the TOMS ozone data. We also thank the two anonymous reviewers for providing several important points for improving this manuscript.

References

Andrews, D. G., J. R. Holton, and C. B. Leovy, *Middle Atmosphere Dynamics*, 489 pp., Academic, San Diego, Calif., 1987.

Appenzeller, C., J. R. Holton, and K. H. Rosenlof, Seasonal variation of mass transport across the tropopause, *J. Geophys. Res.*, *101*, 15,071–15,078, 1996.

Beekmann, M., et al., Regional and global tropopause fold occurrence and related ozone flux across the tropopause, *J. Atmos. Chem.*, *28*, 29–44, 1997.

Bertin, F., B. Camistron, and J. L. Caccia, Mixing processes in a tropopause folding observed by an network of ST radar and lidar, *Ann. Geophys.*, *19*, 953–963, 2001.

Bey, I., et al., Global modeling of tropospheric chemistry with assimilated meteorology: Model description and evaluation, *J. Geophys. Res.*, *106*, 23,073–23,095, 2001.

Bruhl, C., et al., Halogen Occultation Experiment ozone channel validation, *J. Geophys. Res.*, *101*, 10,217–10,240, 1996.

Brunner, D., J. Staehelin, D. Jeker, H. Wernli, and U. Schumann, Nitrogen oxides and ozone in the tropopause region of the Northern Hemisphere: Measurements from commercial aircraft in 1995/1996 and 1997, *J. Geophys. Res.*, *106*, 27,673–27,700, 2001.

Chandra, S., J. R. Ziemke, W. Min, and W. G. Read, Effects of 1997–1998 El Niño on tropospheric ozone and water vapor, *Geophys. Res. Lett.*, *25*, 3867–3870, 1998.

Chandra, S., J. R. Ziemke, and R. W. Stewart, An 11-year solar cycle in tropospheric ozone from TOMS measurements, *Geophys. Res. Lett.*, *26*, 185–188, 1999.

Chandra, S., J. R. Ziemke, P. K. Bhartia, and R. V. Martin, Tropical tropospheric ozone: Implications for dynamics and biomass burning, *J. Geophys. Res.*, *107*(D14), 4188, doi:10.1029/2001JD00044, 2002.

Chandra, S., J. R. Ziemke, and R. V. Martin, Tropospheric ozone at tropical and middle latitudes derived from TOMS/MLS residual: Comparison with a global model, *J. Geophys. Res.*, *108*(D9), 4291, doi:10.1029/2002JD002912, 2003.

Cho, J. Y. N., et al., Observations of convective and dynamical instabilities in tropopause folds and their contribution to stratosphere-troposphere exchange, *J. Geophys. Res.*, *104*, 21,549–21,568, 1999.

Eck, T. F., P. K. Bhartia, P. H. Hwang, and L. L. Stowe, Reflectivity of Earth's surface and clouds in ultraviolet from satellite observations, *J. Geophys. Res.*, *92*, 4287–4296, 1987.

Eisele, H., H. E. Scheel, R. Sladkovic, and T. Trickl, High-resolution lidar measurements of stratosphere-troposphere exchange, *J. Atmos. Sci.*, *56*, 319–330, 1999.

Fishman, J., and A. E. Balok, Calculation of daily tropospheric ozone residuals using TOMS and empirically improved SBUV measurements: Application to an ozone pollution episode over the eastern United States, *J. Geophys. Res.*, *104*, 30,319–30,340, 1999.

Fishman, J., and J. C. Larsen, Distribution of total ozone and stratospheric ozone in the tropics: Implications for the distribution of tropospheric ozone, *J. Geophys. Res.*, *92*, 6627–6634, 1987.

Fishman, J., C. E. Watson, J. C. Larsen, and J. A. Logan, Distribution of tropospheric ozone determined from satellite data, *J. Geophys. Res.*, *95*, 3599–3617, 1990.

Fujiwara, M., and M. Takahashi, Role of the equatorial Kelvin wave in stratosphere-troposphere exchange in a general circulation model, *J. Geophys. Res.*, *106*, 22,763–22,780, 2001.

Hudson, R. D., and A. M. Thompson, Tropical tropospheric ozone (TTO) from TOMS by a modified-residual method, *J. Geophys. Res.*, *103*, 22,129–22,145, 1998.

Jiang, Y., and Y. L. Yung, Concentrations of tropospheric ozone from 1979 to 1992 over tropical Pacific South America from TOMS data, *Science*, *272*, 714–716, 1996.

Joiner, J., and P. K. Bhartia, The determination of cloud pressures from rotational Raman scattering in satellite backscatter ultraviolet measurements, *J. Geophys. Res.*, *100*, 23,019–23,026, 1995.

Kim, J. H., and M. J. Newchurch, Climatology and trends of tropospheric ozone over the eastern Pacific Ocean: The influences of biomass burning and tropospheric dynamics, *Geophys. Res. Lett.*, *23*, 3723–3726, 1996.

Kim, J. H., M. J. Newchurch, and K. Han, Distribution of tropical tropospheric ozone determined by the scan-angle method applied to TOMS measurements, *J. Atmos. Sci.*, *58*, 2699–2708, 2001.

Langford, A., et al., Ozone measurements in a tropopause fold associated with a cut-off low system, *Geophys. Res. Lett.*, *23*, 2501–2504, 1996.

Lelieveld, J., and F. J. Dentener, What controls tropospheric ozone?, *J. Geophys. Res.*, *105*, 3531–3551, 2000.

Liu, S., et al., Sources of reactive nitrogen in the upper troposphere during SONEX, *Geophys. Res. Lett.*, *26*, 2441–2444, 1999.

Logan, J. A., An analysis of ozonesonde data for the troposphere: Recommendations for testing three-dimensional models and development of a gridded climatology for tropospheric ozone, *J. Geophys. Res.*, *104*, 16,115–16,150, 1999.

Marenco, A., et al., Measurement of ozone and water vapor by Airbus in-service aircraft: The MOZAIC airborne program, an overview, *J. Geophys. Res.*, *103*, 25,631–25,642, 1998.

Martin, R. V., D. J. Jacob, J. A. Logan, J. R. Ziemke, and R. Washington, Detection of lightning influence on tropical tropospheric ozone, *Geophys. Res. Lett.*, *27*, 1639–1642, 2001.

Martin, R., et al., Interpretation of TOMS observations of tropical tropospheric ozone with a global model and in situ observations, *J. Geophys. Res.*, *107*(D18), 4351, doi:10.1029/2001JD001480, 2002.

Meloen, J., P. C. Siegmund, and M. Sigmond, A Lagrangian computation of stratosphere-troposphere exchange in a tropopause folding event in the subtropical Southern Hemisphere, *Tellus, Ser. A*, *53*, 368–379, 2001.

Moxim, W., and J. Levy II, A model analysis of tropical South Atlantic Ocean tropospheric ozone maximum: The interaction of transport and chemistry, *J. Geophys. Res.*, *105*, 17,393–17,415, 2000.

Newchurch, M. J., D. Sun, and J. H. Kim, Zonal wave-1 structure in TOMS tropical stratospheric ozone, *Geophys. Res. Lett.*, *28*, 3151–3154, 2001.

Randel, W. J., Global atmospheric circulation statistics, 1000-1 mb, *Tech. Note TN-366+STR*, 256 pp., Natl. Cent. for Atmos. Res., Boulder, Colo., 1992.

Sudo, K., and M. Takahashi, Simulation of tropospheric ozone changes during 1997–1998 El Nino: Meteorological impact on tropospheric photochemistry, *Geophys. Res Lett.*, *28*, 4091–4094, 2001.

Thompson, A. M., and R. D. Hudson, Tropical tropospheric ozone (TTO) maps from Nimbus 7 and Earth Probe TOMS by the modified-residual method: Evaluation with sondes, ENSO signals, and trends from Atlantic regional time series, *J. Geophys. Res.*, *104*, 26,961–26,975, 1999.

Vukovich, F., M. Brackett, V. Fishman, and J. E Sickles II, On the feasibility of using the tropospheric ozone residual for nonclimatological studies on a quasi-global scale, *J. Geophys. Res.*, *101*, 9093–9105, 1996.

Wang, Y., D. J. Jacob, and J. A. Logan, Global simulation of tropospheric O_3-NO_x-hydrocarbon chemistry: 1. Model formulation, *J. Geophys. Res.*, *103*, 10,713–10,725, 1998.

Ziemke, J. R., and S. Chandra, Seasonal and interannual variabilities in tropical tropospheric ozone, *J. Geophys. Res.*, *104*, 21,425–21,442, 1999.

Ziemke, J. R., S. Chandra, and P. K. Bhartia, Two new methods for deriving tropospheric column ozone from TOMS measurements: The assimilated UARS MLS/HALOE and convective-cloud differential techniques, *J. Geophys. Res.*, *103*, 22,115–22,127, 1998.

Ziemke, J. R., S. Chandra, and P. K. Bhartia, "Cloud slicing": A new technique to derive upper tropospheric ozone from satellite measurements, *J. Geophys. Res*, *106*, 9853–9867, 2001.

P. K. Bhartia, S. Chandra, and J. R. Ziemke, NASA Goddard Space Flight Center, Code 916, Building 33, Room 3410, Greenbelt, MD 20771, USA. (ziemke@jwocky.gsfc.nasa.gov)